## eNeuro

Research Article: New Research | Sensory and Motor Systems

### Temporal dynamics of inhalation-linked activity across defined subpopulations of mouse olfactory bulb neurons imaged in vivo

### Shaina M. Short<sup>1</sup> and Matt Wachowiak<sup>1</sup>

<sup>1</sup>Department of Neurobiology and Anatomy, University of Utah, Salt Lake City, UT 84112, USA

https://doi.org/10.1523/ENEURO.0189-19.2019

Received: 16 May 2019

Accepted: 23 May 2019

Published: 17 June 2019

Author contributions: S.M.S. and M.W. designed research; S.M.S. performed research; S.M.S. and M.W. analyzed data; S.M.S. and M.W. wrote the paper.

Funding: HHS | NIH | National Institute on Deafness and Other Communication Disorders (NIDCD) F32DC016531

R01DC006441

Conflict of Interest: Authors report no conflict of interest.

This work was supported by the National Institute on Deafness and Other Communication Disorders [F32DC016531 to S.M.S, R01DC006441 to M.W.].

Correspondence to be sent to Shaina M. Short at shaina.short@utah.edu.

Cite as: eNeuro 2019; 10.1523/ENEURO.0189-19.2019

Alerts: Sign up at www.eneuro.org/alerts to receive customized email alerts when the fully formatted version of this article is published.

Accepted manuscripts are peer-reviewed but have not been through the copyediting, formatting, or proofreading process.

Copyright © 2019 Short and Wachowiak

This is an open-access article distributed under the terms of the Creative Commons Attribution 4.0 International license, which permits unrestricted use, distribution and reproduction in any medium provided that the original work is properly attributed.

- 2 Temporal dynamics of inhalation-linked activity across defined subpopulations of mouse
- 3 olfactory bulb neurons imaged in vivo
- 4 2. Abbreviated Title (50 character maximum)
- 5 Temporal dynamics of olfactory bulb neurons
- 6 3. List all Author Names and Affiliations in order as they would appear in the published ar 7 ticle
- 8 Shaina M. Short<sup>1</sup>, Matt Wachowiak<sup>1</sup>
- <sup>1</sup>Department of Neurobiology and Anatomy, University of Utah, Salt Lake City, UT 84112, USA
- 10 4. Author Contributions: Each author must be identified with at least one of the following:
- 11 Designed research, Performed research, Contributed unpublished reagents/ analytic
- 12 tools, Analyzed data, Wrote the paper.
- 13 SMS and MW Designed research; SMS Performed research; SMS and MW Analyzed data;
- 14 SMS and MW Wrote the paper 15

### 16 5. Correspondence should be addressed to (include email address)

- 17 Correspondence to be sent to: Shaina M. Short, Department of Neurobiology and Anatomy,
- 18 University of Utah, Salt Lake City, UT, USA. email: shaina.short@utah.edu
- 19 6. Number of Figures: 7
- 20 **7. Number of Tables:** 0
- 21 8. Number of Multimedia: 0
- 22 9. Number of words for Abstract: 250
- 23 **10. Number of words for Significance Statement:** 119
- 24 **11. Number of words for Introduction:** 620
- 25 **12. Number of words for Discussion:** 1488
- 26 13. Acknowledgements: We thank Jackson Ball, Rebecca L. Kummer, and Gustavo A.
- 27 Vasquez-Opazo for excellent technical assistance, Thomas Rust for data analysis software and
- Tom P. Eiting, Shawn D. Burton, Isaac A. Youngstrom, Yusuke Tsuno, and Andrew K. Moran for helpful feedback and discussion.

### 30 14. Conflict of Interest

31 Authors report no conflict of interest

### 32 15. Funding sources

- 33 This work was supported by the National Institute on Deafness and Other Communication
- 34 Disorders [F32DC016531 to S.M.S, R01DC006441 to M.W.].

35

36

37

38

39

## Temporal dynamics of inhalation-linked activity across defined subpopulations of mouse olfactory bulb neurons imaged in vivo

43

### 44 ABSTRACT

45 In mammalian olfaction, inhalation drives the temporal patterning of neural activity that underlies early olfactory processing. It remains poorly understood how the neural circuits that process 46 47 incoming olfactory information are engaged in the context of inhalation-linked dynamics. Here, 48 we used artificial inhalation and two-photon calcium imaging to compare the dynamics of activity 49 evoked by odorant inhalation across major cell types of the mouse olfactory bulb (OB). We 50 expressed GCaMP6f or jRGECO1a in mitral and tufted cell subpopulations, olfactory sensory 51 neurons, and two major juxtaglomerular interneuron classes, and imaged responses to a single 52 inhalation of odorant. Activity in all cell types was strongly linked to inhalation, and all cell types 53 showed some variance in the latency, rise-times, and durations of their inhalation-linked 54 response. Juxtaglomerular interneuron dynamics closely matched that of sensory inputs, while 55 mitral and tufted cells showed the highest diversity in responses, with a range of latencies and 56 durations that could not be accounted for by heterogeneity in sensory input dynamics. Diversity 57 was apparent even among 'sister' tufted cells innervating the same glomerulus. Surprisingly, 58 inhalation-linked responses of mitral and tufted cells were highly overlapping and could not be 59 distinguished on the basis of their inhalation-linked dynamics, with the exception of a 60 subpopulation of superficial tufted cells expressing cholecystokinin. Our results are consistent 61 with a model in which diversity in inhalation-linked patterning of OB output arises first at the level of sensory input and is enhanced by feedforward inhibition from juxtaglomerular interneurons 62 which differentially impact different subpopulations of OB output neurons. 63

64

### 65 SIGNIFICANCE STATEMENT

66 Inhalation drives the temporal patterning of neural activity that underlies olfactory processing and rapid odor perception, yet the dynamics of the neural circuit elements mediating this 67 68 processing are poorly understood. By comparing inhalation-linked dynamics of major olfactory 69 bulb subpopulations, we find that diversity in the timing of neural activation arises at the level of 70 sensory input, which is then mirrored by inhibitory interneurons in the glomerular layer. 71 Temporal diversity is higher among olfactory bulb output neurons, with different subpopulations 72 showing distinct but nonetheless highly overlapping ranges of inhalation-linked dynamics. These 73 results implicate feedforward inhibition by glomerular-layer interneurons in diversifying temporal 74 responses among output neurons, which may be important for generating and shaping timing-75 based odor representations during natural odor sampling.

76

### 77 INTRODUCTION

78 Temporal patterning of neural activity is a fundamental aspect of information coding and 79 processing by neural circuits. In the mammalian olfactory system, the primary driver of 80 temporally patterned activity is inhalation of air through the nasal cavity. Inhalation delivers 81 transient pulses of odorant to the olfactory epithelium, and so determines the initial temporal 82 structure of olfactory sensory input to the brain and drives the temporal patterning of activity at 83 subsequent processing stages (Macrides and Chorover, 1972, Onoda and Mori, 1980, Sobel 84 and Tank, 1993, Kepecs et al., 2006, Schaefer et al., 2006, Schaefer and Margrie, 2007, 85 Wachowiak, 2011). Behavioral and psychophysical studies have shown that odor percepts are formed within the time of a single inhalation (150-250 ms for rodents, ~400 ms for humans) 86 87 (Laing, 1986, Johnson et al., 2003, Kepecs et al., 2007), and neurophysiological studies have 88 demonstrated that the temporal pattern of neural activity elicited by a single inhalation of odorant 89 can robustly encode odorant identity and intensity (Uchida and Mainen, 2003, Kepecs et al., 90 2007, Wesson et al., 2008, Wesson et al., 2009, Cury and Uchida, 2010, Shusterman et al.,

2011, Rebello et al., 2014). Thus, understanding how inhalation-linked temporal patterns of
activity are generated and shaped by neural circuits in the early olfactory pathway is
fundamental to understanding olfactory information processing.

94 Neural circuits in the olfactory bulb (OB) mediate the first steps in processing olfactory 95 inputs: here, olfactory sensory neurons (OSNs) drive excitation of mitral and tufted cells (MTCs), 96 the principal output neurons of the OB, as well as activate multiple inhibitory circuits within and 97 between OB glomeruli (Wachowiak and Shipley, 2006). This juxtaglomerular inhibition is 98 hypothesized to play a critical role in shaping MTC responses to odorants (Gire and Schoppa, 99 2009, Shao et al., 2009, Shao et al., 2012, Fukunaga et al., 2014, Banerjee et al., 2015, Liu et 100 al., 2016b) yet the temporal dynamics of activity among different juxtaglomerular interneurons 101 with respect to inhalation have not been well-characterized. Two types of juxtaglomerular 102 interneuron classes – periglomerular (PG) and short axon (SA) cells – are hypothesized to 103 mediate feedforward and lateral inhibition, respectively, with differential impacts on the temporal 104 dynamics of MTC responses (Aungst et al., 2003, Shao et al., 2009, Shirley et al., 2010, 105 Fukunaga et al., 2012, Shao et al., 2012, Liu et al., 2013, Whitesell et al., 2013, Banerjee et al., 106 2015, Najac et al., 2015, Liu et al., 2016b, Geramita and Urban, 2017). Additionally, feedback 107 inhibition mediated by reciprocal connections between MTCs to PG or SA cells may also shape 108 MTC temporal patterning (Najac et al., 2015).

Here, we sought to better characterize the temporal dynamics of inhalation-driven activity among major circuit elements in the OB in order to refine models of OB circuit function during naturalistic odorant sampling in vivo. We used cell-type specific imaging with GCaMP-based reporters to record from different subpopulations of MTCs as well as presumptive PG cells, SA cells, and OSN inputs. We used an artificial inhalation paradigm to examine responses to a single inhalation of odorant with high fidelity and to precisely compare inhalation-linked response patterns across experiments and between cell types. We found distinct differences in

116 the inhalation-linked temporal patterns of activity among different cell types, with PG and SA cell 117 populations showing faster responses to inhalation than either mitral or tufted cells, and a range 118 of excitatory MTC response dynamics that could not be accounted for by diversity in the 119 dynamics of OSN inputs. At the same time, we observed a great deal of overlap in the 120 inhalation-linked temporal patterns of activity among superficial tufted and mitral cells. Overall, 121 these results support circuit models in which juxtaglomerular interneurons mediate rapid 122 feedforward inhibition that contributes to diverse inhalation-linked temporal patterning in both 123 mitral and tufted cells.

124

### 125 MATERIALS AND METHODS

126

127 Animals. Genetically-engineered mice expressing Cre recombinase (Cre) targeted to specific 128 neuronal populations were used for experiments. Mice were either crossed to the Ai95 129 GCaMP6f reporter line (The Jackson Laboratory (JAX), stock #024105) or injected with a viral 130 vector. The mouse strains using included GAD2-IRES-Cre mice (JAX Stock #010802), TH-Cre 131 (JAX stock #008601), DAT-IRES-Cre mice (JAX stock #006660), OMP-Cre (JAX stock 132 #006668), PCdh21-Cre (Gensat stock# 030952-UCD) (Nagai et al., 2005), Tbet-Cre (JAX stock 133 #024507), Thy1-GCaMP6f transgenic mice (JAX stock #024339, line GP5.11) mice, and CCK-134 IRES-CRE (JAX stock #012706). Mice were on average 4.6 months of age by completion of 135 data collection. Both female (46) and male (54) mice were used. Mice were housed up to 5 per 136 cage in a 12/12h light/dark cycle. Food and water were provided ad libitum. Each procedure was 137 performed following the National Institutes of Health Guide for the Care and Use of Laboratory 138 Animals and approved by the University of Utah institutional animal care and use committee. 139

142 hSyn.Flex.NES.jRGECO1a.WPRE.SV40) was achieved with the injection of viral vectors. All 143 viruses were obtained from the University of Pennsylvania Viral Vector Core. Injections were 144 made into the dorsal OB under isoflurane anesthesia (0.5-2% in  $O_2$ ). Where applicable, mice 145 used for virus injection were homozygous for the allele driving Cre expression. Using a 146 stereotaxic head holder and drill, a small craniotomy (0.5-1mm) was made on the dorsal surface 147 of the OB. A glass pipette was lowered to a depth 50-150 µm to target periglomerular or short 148 axon interneurons or 200-400 µm to target mitral and tufted cell populations. Mice were single 149 housed following the surgery and imaged 14 - 28 d after injection.

150

151 **In vivo imaging.** Two-photon imaging was performed in acutely anesthetized mice. Initially, 152 pentobarbital (50 mg/kg) was used during the implantation of a double tracheotomy (Wachowiak 153 and Cohen, 2001, Bozza et al., 2004, Spors et al., 2006), after which isoflurane (0.5 - 2% in O<sub>2</sub>) 154 was delivered directly to the tracheotomy tube, bypassing the nose. By controlling negative 155 pressure through the sniff tube, each inhalation lasted exactly 150 ms and had a flow rate of 150 156 ml/min (300 ml/min for two nostrils). The onset of each inhalation was set to occur every 4 s 157 (0.25 Hz), which enabled individual inhalation evoked calcium transients to be averaged. Next, a 158 custom head bar was implanted, a craniotomy was made, and a coverslip was implanted using 159 2.5% low-melting-point agarose over the dorsal OB for imaging (Wachowiak et al., 2013). 160 Throughout surgeries and while imaging, the body temperature was maintained at 37°C with a 161 heating pad and the heart rate at ~400 beats per minute.

Imaging data were collected using either a Moveable Optical Microscope (Sutter
Instruments) coupled to a Mai Tai HP pulsed Ti:Sapphire laser (Newport Corp.) and controlled
by Scanimage 5.1 (Pologruto et al., 2003), or a Neurolabware microscope coupled to a

Cameleon Ultrall laser (Coherent) and controlled by Scanbox software. Both setups used resonance-based scanning and GaAsP photomultipliers (Hamamatsu H10770B) for light collection, and images were collected at a frame rate of 15.5 Hz. A 16X 0.8 N.A. (Nikon) objective was used in all experiments. For dual-color imaging, a Fidelity 1070 nm femtosecond laser was used simultaneous with 920 nm illumination and emission filters were used to separate green (520/65 nm) and red (641/75 nm) emission (Sun et al., 2017). The average power delivered to the sample during imaging was 20 - 60 mW.

172

173 Analysis of imaging data. Maps of inhalation-triggered fluorescence changes (i.e., ITA 174 response  $\Delta F$  maps) were generated by choosing 15 frames before and after odorant inhalation. 175 Imaging trials consisted of three periods of odorant presentation, each lasting 20 sec (i.e., 5 176 inhalations at 0.25 Hz), with a 32 sec interval between presentations. Responses to inhalation of 177 clean air were taken from the last 10 inhalations from the inter-stimulus period in order to ensure 178 that all odorant had cleared from the nose following the stimulus presentation. Note, small transients that immediately followed odor stimulation (Figure 1C, 7<sup>th</sup> inhalation) likely reflect 179 180 incomplete clearance of odorants from in front of, or inside, the nasal cavity. Responses to 181 inhalation of clean air needed to be consistent across inter-stimulus periods of subsequent trials 182 of odorant or a blank (medium-chain triglycerides) no-odor control presentations for the cell to 183 be counted as responding to inhalation alone. For display, ITA response maps were smoothed 184 with a Gaussian filter with sigma 1.25 pixels. Regions of interest (ROIs) were selected manually 185 from ITA response maps or from resting fluorescence images. Fluorescence time series were 186 extracted by averaging all pixels in a ROI using custom MATLAB scripts. All time series data 187 were sampled to 150 Hz using the Matlab piecewise cubic interpolation functions interp1 and 188 pchip. In all cases,  $\Delta F/F$  was calculated as  $(\Delta F/F=(F-F_o)/F_o)$ , with  $F_o$  being the mean 189 fluorescence prior to the inhalation, averaged for each inhalation. However, for population level

analyses, signals were averaged across three trials of 20s odorant presentations (Figure 1).
Excitatory events were defined as ITA responses that were greater than 4 standard deviations
(SD) above the ITA baseline signal, which was defined as 1 second prior to inhalation, whereas
inhibitory events were defined as ITA responses reaching more than 3 SD below baseline.

194

195 Analysis of temporal dynamics. Onset latency was calculated as the first time point in which 196 the following 4 frames of an ITA trace were above the threshold for a significant excitatory 197 response (4 SD above baseline, which was taken from a 1 s pre-stimulus window). Peak 198 response amplitudes and time to peak values were calculated from ITAs that were filtered using 199 a Gaussian-weighted moving average filter with a window length of 270 ms. From this filtered 200 trace, response duration was calculated as the time from 50% of peak response on the rising 201 slope of the signal to 50% of peak on the decaying slope of the signal. Time to peak was 202 calculated from the maximum value of the filtered trace. For pseudo-color plots of ITA 203 responses (e.g., Figure 2C), the mean of the 1-sec pre-stimulus window was subtracted from 204 the response time series and smoothed using a Gaussian filter with a window length of 100ms; 205 the resulting trace was normalized to its own maximum and negative maximum amplitudes for 206 pseudo-color display.

207

Experimental Design and Statistical Tests. Statistical details of experiments are listed in the Results section. All datasets (onset latency, time to peak, and half width response durations across all sTC, MC, OSN, PG, and SA cell populations) rejected the null hypothesis for onesample Kolmogorov-Smirnov test for normality, therefore non parametric statistical tests were performed as stated throughout the methods. A Wilcoxon signed rank test tested was used for paired comparisons across two groups (mitral and tufted cell populations Figure 3), Mann-Whitney U-test was used for unpaired comparisons across two groups (mitral and tufted cell

population Figure 2), and the Kruskal-Wallis test was used for comparisons across all
subpopulation (Figure 6). Post hoc multiple comparisons were performed using Tukey's honest
significant difference criterion (Figure 6). For comparisons of glomerular neuropil dynamics to
PG and sTC somatic responses (e.g., Figure 7), an unpaired ttest was used to statistically
compare standard deviation across sTC and PG glomerulus-cell pairs. All statistical tests were
performed in Matlab. Statistical significance was set at p<0.05 for all tests.</li>

222

221

223 Olfactometry. A custom olfactometer controlled by Labview software was used to present 224 odorants, as previously described (Bozza et al., 2004, Verhagen et al., 2007). Odorant 225 concentration was controlled by diluting from saturated vapor in filtered, ultra-pure air. Odorants 226 were present for 20 sec at 1-5% saturated vapor. Each odorant presentation was separated by 227 a 32s inter-stimulus interval. Odorants were obtained at 95-99% purity (Sigma-Aldrich) and 228 stored under nitrogen. Some odorants were diluted in mineral oil to achieve final concentrations 229 at the animal's nose of 1-20 ppm at 1% saturated vapor. Odorants tested included ethyl 230 butyrate, methyl valerate, butyl acetate, 2-hexanone, ethyl tiglate, 2-methyl pentanal, 2-231 hydroxyacetophenone, and hexyl acetate. Odorants were delivered 0.5 - 1.0 cm in front of the 232 mouse's nose. Filtered, ultra-pure air was delivered to the mouse's nose in between odorant 233 presentations. A fan positioned behind the animal scavenged excess odorant in the room. 234

Histology. An overdose of sodium pentobarbital was used to deeply anesthetize mice prior to
perfusion with phosphate-buffered saline (PBS) followed by 4% paraformaldehyde in PBS.
Overnight, heads were post fixed in 4% paraformaldehyde in PBS. Next, the brain was extracted
and embedded in 5% agarose. Coronal sections (100-200 µm thick) were made with a
Vibratome and mounted onto a glass coverslip before imaging with a Fluoview FV1000 Olympus

240 confocal microscope at 10X, 20X, and 40X magnification.

241

### 242 **RESULTS**

243 To compare the dynamics of inhalation-driven activity across different OB neuron 244 populations, we used an artificial inhalation paradigm that allowed for precise comparison of 245 temporal response dynamics across experiments, as described previously (Wachowiak et al., 246 2013, Diaz-Quesada et al., 2018) (Figure 1 A). We generated single inhalations at 0.25 Hz to 247 enable inhalation-triggered averaging of responses with, in most cases, minimal adaptation from 248 one inhalation to the next. However, the duration and peak flow rate of each inhalation was 249 chosen to be within the range that occurs in awake, freely-breathing mice. We expressed 250 calcium sensors (typically GCaMP6f) in distinct genetically-defined cell types using either viral 251 vectors or genetic expression strategies, and imaged activity from the somata of the targeted 252 cell types or from glomerular neuropil using two-photon laser scanning microscopy (Figure 1B). 253 A typical imaging epoch consisted of three periods of odorant presentation, each lasting 20 254 seconds (i.e., 5 inhalations at 0.25 Hz), with a 32 sec interval between presentations (Figure 255 1C), yielding a total of 15 inhalations in the presence of odorant. We analyzed response 256 dynamics from inhalation-triggered average traces (ITAs) and determined response magnitudes, 257 latencies, and durations, as done previously (Carey et al., 2009)(Figure 1D).

258

259 Inhalation-linked dynamics of mitral/tufted cell subpopulations.

We first examined inhalation-linked response dynamics in mitral and tufted cells (MTCs). Electrophysiological recordings have shown diverse inhalation-linked temporal patterns among MTCs and distinct differences between these subpopulations as defined by soma depth (Fukunaga et al., 2012, Igarashi et al., 2012). To test if these differences were reflected in inhalation-linked calcium signals, we selectively expressed GCaMP6f in MTCs via several

265 mechanisms: viral injection (AAV.Flex.GCaMP6f) into the OB of mice expressing Cre-266 recombinase in protocadherin-21 positive (PCdh21-Cre) neurons (Wachowiak et al., 2013); 267 crossing a Cre-dependent GCaMP6f reporter line with mice expressing Cre in Tbx21-positive 268 (Tbet-Cre) neurons (Haddad et al., 2013) or in cholecystokinin-positive (CCK+) neurons 269 (Seroogy et al., 1985); and use of a transgenic mouse line (Thy1-GCaMP6f) selective for 270 expression in MTCs (Dana et al., 2014). Patterns of GCaMP6f expression using PCdh21-Cre, 271 Tbet-Cre, or Thy1-GCaMP6f mice were qualitatively similar, as described previously 272 (Wachowiak et al., 2013) with expression in large numbers of MTCs (Figure 2A). To compare 273 mitral and tufted cells, we distinguished each population by somatic depth (Figure 2B). We 274 restricted our analysis to somata that were clearly in the mitral cell layer (MCs) and superficial 275 tufted cells (sTCs) just below the glomerular layer, excluding deeper or middle tufted cells in the 276 external plexiform layer.

277 For both MCs and sTCs, the predominant inhalation-linked response pattern was a 278 transient fluorescence increase, presumably corresponding to a brief spike burst after inhalation. 279 There was substantial diversity in the dynamics of this transient, with different cells showing 280 differences in onset latency, time to peak response, and response duration; such diversity was 281 apparent for different cells of the same type (i.e., sTCs or MCs) imaged within the same 282 preparation during the same odorant presentation (Figure 2B). When comparing only excitatory 283 responses, MCs and sTCs showed statistically significant differences in latency, time to peak, and response duration (p = 0.0032, 0.0119 and  $3.3e^{-9}$  respectively. Mann-Whitney U test, 284 285 MC=86 cell-odor pairs from 5 mice, sTC=218 cell-odor pairs from 16 mice), their response 286 dynamics were highly overlapping (Figure 2C, D). MCs and sTCs differed most substantially in 287 their response durations, with MCs showing significantly longer-duration responses (median, 288 1309 ms, interguartile range: 892 – 1994 ms) compared to sTCs (median, 788 ms, interguartile 289 range: 611 – 1296 ms, Figure 2E). Another difference observed between sTCs and MCs was

their responsiveness to inhalation of clean air: 9.5% of sTCs (22/231 cells tested with clean air)
and zero MCs (0/89 cells tested) showed a significant response to inhalation of clean air.

292 In several cases we were able to more directly compare sTC and MC response 293 dynamics, either by imaging sTCs and MCs in the same field of view using an oblique imaging 294 plane (n = 3 fields of view from 2 mice) (Figure 3A) or by imaging sTC and MC responses to the 295 same odorant in successive trials by shifting the focal plane from the superficial external 296 plexiform layer to the mitral cell layer (n = 3 paired imaging planes from 2 mice). Even with this 297 within-preparation comparison, sTC and MC response dynamics were still highly overlapping 298 (Figure 3B). There was no significant difference in the median ITA onset latency when 299 comparing MC and sTC populations within the same preparation or field of view (Figure 3C, left 300 panel, Wilcoxon signed rank test, p=0.16, n = 6 paired comparisons, 58 total MCs, 38 total 301 sTCs). Likewise, there was no significant difference in median sTC and MC ITA time to peak 302 (Figure 3C, middle panel, Wilcoxon signed rank test p=0.22). However, the median half width 303 durations of sTC responses were significantly shorter compared to MC responses (Figure 3C, 304 right panel, Wilcoxon signed rank test p=0.03). This analysis supports the conclusion that, as a 305 population, sTCs show slightly shorter-duration responses than MCs, but that individual sTCs 306 and MCs overlap substantially in their inhalation-linked response dynamics.

307 Finally, we measured inhalation-linked responses in sTCs defined by their expression of 308 the peptide transmitter cholecystokinin (CCK), which likely constitute a subset of Tbx21+, 309 Thy1+, or PCdh21+ sTCs (Seroogy et al., 1985, Liu and Shipley, 1994, Tobin et al., 2010) and 310 have previously shown to exhibit shorter-onset and simpler odorant-evoked responses than 311 MCs (Economo et al., 2016). Consistent with these earlier reports, sTCs imaged from 312 GCaMP6f:CCK-Cre mice (n= 52 cell-odor pairs in 3 mice) indeed showed onset latencies that 313 were, as a population, significantly shorter than those of MCs (p = 3.7e-5) or the general sTC 314 population (p = 0.0333) defined by Tbx21, PCdh21, or Thy1 expression (median onset latency:

315 247 ms, interguartile range: 206-311 ms; Mann-Whitney test, Figure 2C-E). Over a guarter of 316 the slowest sTCs onset latencies were slower than 90% of that of the CCK+ sTC population 317 (Figure 2E). Likewise, CCK+ sTCs showed an earlier time-to-peak than the general sTC 318 population (p = 0.0022, Mann-Whitney test). CCK+ sTCs showed the largest difference in their 319 response durations, which were uniformly short (median, 635 ms, range: 520 - 735 ms) and significantly shorter than the general sTC population ( $p = 9.1e^{-5}$ , Mann-Whitney test). Thus, 320 321 CCK+ sTCs appear to constitute a distinct subpopulation of sTCs with more rapid inhalation-322 triggered response patterns.

323 We also examined inhalation-linked suppression in MTCs. Previous reports indicate that 324 about a third of MTCs show odorant-evoked suppression of ongoing activity (Kollo et al., 2014, 325 Economo et al., 2016, Diaz-Quesada et al., 2018). We assessed whether phasic suppression 326 elicited by each inhalation was apparent in GCaMP6f signals, using a conservative criterion of a 327 fluorescence decrease in the ITA of at least 3 SD below the pre-inhalation baseline. Using these 328 criteria, odorant-evoked, inhalation-linked suppression was sparsely distributed and relatively 329 rare (Figure 4A), with only 8 of 93 (9%) of all MC-odor pair responses and 5 of 240 (2%) of all 330 sTC-odor pair responses showing suppressive ITAs. Note for these comparisons cell-odor pairs 331 include all responses that were either significantly excited or suppressed. This prevalence is 332 substantially smaller than the prevalence of suppressive responses seen in awake, freely-333 breathing mice or during higher-frequency (2 Hz) artificial inhalation (Economo et al., 2016), or 334 as measured with whole-cell recordings (Kollo et al., 2014, Diaz-Quesada et al., 2018). A 335 possible explanation for this difference is that the ability to detect inhalation-linked suppression 336 using the GCaMP6f reporter was clearly dependent on baseline activity levels in individual cells, 337 which could fluctuate over the course of a trial (Figure 4A). Notably, both MCs and sTCs could 338 also show phasic suppression linked to inhalation of clean air alone (example sTC Figure 4B). 339 When looking across all recorded cells, suppression more prevalent among sTCs than MCs (21

of 231 sTCs versus 2 of 89 MCs). Even in these cases, however, inhalation-linked suppression
was sparsely distributed among the multiple cells in a field of view (Figure 4B).

342 Overall, these data suggest that the chief difference in the inhalation-triggered dynamics 343 of MCs versus sTCs is that MCs show a greater range of excitatory response latencies and 344 durations than do sTCs. At the same time, they also suggest that sTC and MC responses do not 345 unambiguously map to any single parameter of the inhalation-linked response, including 346 response latency, response duration, or even response polarity. This finding does not contradict 347 recent work which found that inhalation of clean air evokes distinct temporal dynamics across 348 MC and TC populations (Fukunaga et al., 2012, Fukunaga et al., 2014), as our results shown 349 here are specific to inhalation driven dynamics in the presence of odorant. However, responses 350 to clean air were rare in this study and thus we could not reliably compare latencies to 351 corroborate these earlier findings. We next used this same approach to gain insight into where 352 in the OB circuit the diversity in response patterns might arise by imaging inhalation-triggered 353 responses from olfactory sensory neurons (OSNs) and juxtaglomerular interneurons.

354

355 Contribution of olfactory sensory input dynamics to MTC response diversity.

356 One determinant of diverse MT cell inhalation-linked response dynamics could be 357 diversity in the temporal patterns of sensory input to the OB (Spors et al., 2006). To assess this 358 we measured the temporal dynamics of OSN input to OB glomeruli using GCaMP6f expressed 359 in OSNs (Figure 5A) and imaging responses from OSN axon terminals, as described previously 360 (Wachowiak et al., 2013). Consistent with earlier studies (Spors et al., 2006, Carey et al., 2009, 361 Wachowiak et al., 2013), OSN responses were predominately simple transient fluorescence 362 increases following each inhalation (Figure 5B-D). Surprisingly, inhalation of clean air elicited 363 significant excitatory responses in only 1 of 72 glomeruli imaged (1/72), a lower fraction than 364 expected given prior reports of inhalation-linked excitation among OSNs (Grosmaitre et al.,

2007, Carey et al., 2009). We also observed inhalation-linked suppressive responses in a small
fraction (3/72) of glomeruli imaged.

367 With respect to odorant-evoked activity, OSN ITAs varied in their latency of onset, rise-368 time and response duration, and different odorants could elicit different inhalation-triggered 369 dynamics within the same glomerulus (Figure 5C, D). As a population, OSN response onset 370 latencies were distributed earlier than those of MCs, with 50% of glomerular OSN latencies 371 preceding the shortest 82.6% of MC responses (Figure 5E, F, median, 242 ms, range, 197 - 321 372 ms, n= 88 glomerulus-odor pairs, 5 mice). Qualitatively similar differences in temporal dynamics 373 between OSN and MTC responses appeared for time to peak and response duration, (Figure 374 5F). The largest difference between OSN and MTC ITA dynamics was in the duration of the 375 OSN versus MC responses, with half of all MCs showing ITA durations longer than 72.7% of all 376 OSN responses. Notably, the distributions of onset latencies, rise-times, and durations for OSN 377 inputs overlapped closely with those of CCK+ sTCs (Figure 5F). These results are consistent 378 with a model in which inhalation-linked excitatory responses among sTCs – and in particular, 379 CCK+ sTCs - largely reflect excitatory drive from OSNs, while MC excitation is further shaped by 380 additional synaptic or intrinsic mechanisms (Kikuta et al., 2013, Adam et al., 2014).

381

382 Temporal dynamics of inhalation-linked activity in juxtaglomerular interneurons.

We next characterized inhalation-linked responses in juxtaglomerular interneurons, focusing on periglomerular (PG) and short axon (SA) cells – these two classes of interneurons are hypothesized to shape MTC responses via feedforward and lateral inhibition (Kosaka and Kosaka, 2008, Liu et al., 2013, Fukunaga et al., 2014, Banerjee et al., 2015, Liu et al., 2016a). GCaMP6f was preferentially targeted to PG or SA cells by either virus injection (AAV.Flex.GCaMP6f) or Rosa-GCaMP6f reporter cross using GAD2-Cre mice (for PG cells) or TH-Cre or DAT-Cre mice (for SA cells), as described previously (Wachowiak et al., 2013, Banerjee et al., 2015) (Figure 6A, D). Calcium signals were imaged from somata located around
the glomerulus periphery (Figure 6B, E).

392 Both GAD2+ PG and TH/DAT+ SA cell ITA odor responses consisted overwhelmingly of 393 simple, monophasic response transients; multiphasic responses were not seen (Figure 5C, F). 394 In contrast to MCs and sTCs, odorants did not elicit suppressive responses in 1/145 PG cell-395 odor pairs or 0/132 SA cell-odor pairs. When examining individual cells, clean air did elicit 396 excitatory responses in a small fraction of both cell types (7/136 PG cells; 2/120 SA cells). With 397 respect to odorant-evoked response dynamics, PG and SA cell populations both had short-398 latency ITAs, with the main difference being a 'tail' of longer-latency SA cell responses (Figure 399 5I, J). Indeed, the median PG cell ITA latency preceded that of 94% of all MCs, whereas the 400 median SA cell ITA latency preceded 88% of all MCs. At the population level, OSN inputs, PG, 401 SA cells, and CCK+ sTC all had ITA onset latencies that were statistically similar to each other (Kruskal-Wallis test, Chi-sg=100.45, df=715, P>Chi-sg=4.2e<sup>-20</sup>, Tukey-Kramer post hoc test, 402 403 p>0.05) and significantly faster than that of MCs and other sTCs (Figure 5I, J, left panels, 404 Tukey-Kramer post hoc test, p<0.05). Similar trends were observed when comparing time to 405 peak response across these populations (Figure 5I, J, middle panels, Kruskal-Wallis test, Chisq=162.05, df=715, P>Chi-sq=3.6e<sup>-33</sup>). 406

407 SA cell responses differed from those of PG cells mainly in their response durations 408 (Figure 5I, J, right panels, PG half width median, 646 ms, interguartile range: 504 – 1018 ms, 409 SA median, 935 ms, interguartile range: 566 – 1514 ms), with SA cell durations shifted towards 410 longer values than those of PG cells (Figure 5I, J, right panels). Indeed, there was no significant 411 difference in response duration of OSNs, PG cells, and CCK+ sTCs (Kruskal-Wallis test, Chisq=104.62, df=698, P>Chi-sq=5.6e<sup>-21</sup>, Tukey-Kramer post hoc p>0.05), while SA cell response 412 413 durations were significantly longer than all three of these populations (Tukey-Kramer post hoc 414 p<0.05). Interestingly, SA and sTC response durations were statistically indistinguishable

415 (Tukey-Kramer post hoc p>0.05). The similar inhalation-linked dynamics among these groups, 416 which encompasses axon terminals, small-sized PG somata and larger-sized sTC somata 417 suggests that variation in calcium dynamics, as a function of cellular compartment or soma size 418 is not a major determinant of the response dynamics seen after odorant inhalation. Overall, 419 these results suggest that inhalation-linked PG and SA responses largely follow those of OSN 420 inputs, while a subset of SA cells exhibit longer-lasting responses. Their short onset latencies 421 are consistent with both cell types mediating rapid feedforward inhibition of MCs and sTCs 422 during inhalation.

423

424 The diversity of inhalation-linked response dynamics within a single glomerulus.

425 PG cells, sTCs, and MCs all receive excitatory input from dendrites confined to a single 426 glomerulus, and there is evidence that different MCs associated with the same glomerulus (i.e., 427 sister MCs) can show distinct temporal response patterns (Dhawale et al., 2010, Arneodo et al., 428 2018), while sister PG cells have been reported to show temporally uniform response latencies 429 (Homma et al., 2019). We thus next asked to what degree does variance in inhalation-linked 430 response patterns reflect heterogeneity among sister PG cells or sTCs, as opposed to simply 431 reflecting glomerulus- and odorant-specific diversity in OSN input dynamics (Spors et al., 2006). 432 Initially we directly compared PG and sTC response dynamics during the same odor 433 stimulus and within the same glomerulus using two-color imaging We used Thy1-GCaMP6f: 434 GAD2-Cre crosses, expressing the red shifted calcium indicator jRGECO1a (Dana et al., 2016) 435 in PG cells using a Cre-dependent viral vector (Figure 7A). Separate excitation lasers and 436 selective emission filters (see Methods) were used to simultaneously and selectively image from 437 Thy1+ sTCs and GAD2+ PG cells in the same field of view or from the neuropil of the same 438 glomerulus (Figure 7B). Signals imaged from the glomerular neuropil were generally similar for 439 the Thy1+ signal, which reflected summed activity in mitral as well as tufted cell primary

440 dendrites, and the GAD2+ signal, which reflected summed activity across PG cell processes 441 (Figure 7C, 23 glomeruli, 3 mice). The slower decay in the GAD2+ signal is consistent with the 442 slower decay of jRGECO1a after a calcium transient as compared to GCaMP6f (Dana et al., 443 2016). However, imaging from individual PG and sTC somata associated with the same 444 glomerulus revealed diversity in inhalation-triggered dynamics, with different cells showing 445 distinct time to peak and response durations (Figure 7D). While the numbers of sister PG and 446 sTC cells imaged from the same glomerulus were not sufficient for strong statistical analysis, 447 these observations directly demonstrate that distinct inhalation-triggered temporal dynamics can 448 emerge among different neurons innervating the same glomerulus.

449 To more systematically compare this diversity of PG cells and sTCs, we returned to single-wavelength imaging using GCaMP6f, focusing on collecting data from sister PG (Figure 450 451 6BC) or sTC somata (Figure 7EF) in separate preparations. We assessed heterogeneity among 452 sister cells of each cell type by computing the standard deviation ( $\sigma$ ) of the ITA onset latencies 453 and times to peak across all cells associated with a single 'parent' glomerulus (Figure 7G, H). 454 Onset latencies and times to peak were more variable across sister sTCs than for PG cells: the 455  $\sigma$  for sTC and PG cell of sister sTC onset latencies was 45 ± 9 ms (mean ± s.e.m, n= 14 456 glomeruli from 6 mice) compared with  $19 \pm 0.01$  ms (n=16 glomeruli from 4 mice) for PG cells 457 (p=0.008, unpaired t-test, Figure 7G), consistent with a recent report (Homma et al., 2019); the 458 standard deviation of times to peak (same glomeruli and cells as above) was 123 ± 20 ms for 459 sTCs, compared with 73 ± 36 ms for PG cells (p=0.025, unpaired t-test, Figure 7H). As 460 expected, the variance among sister PG or sTCs was less than the variance across the entire 461 population of imaged neurons ( $\sigma$  for sTC and PG cell onset latencies, 217 msec and 61 msec, 462 respectively;  $\sigma$  for sTC and PG cell times to peak, 430 and 140 msec), but was still substantial. 463 These results suggests that the greater variability in inhalation-triggered response dynamics 464 observed across the population of sTCs as compared to PG cells is not merely an artifact of

eNeuro Accepted Manuscript

sampling across different glomeruli, but instead that this diversity can emerge within theglomerular circuit.

467

### 468 **DISCUSSION**

469 A single inhalation of odorant is sufficient for odor identification, and incoming olfactory 470 information arrives at the olfactory bulb in the form of transient bursts of OSN activity linked to 471 each inhalation. The neural circuits that process olfactory inputs are well known, but how these 472 circuits respond to the dynamic inputs driven by odorant inhalation in vivo remains unclear. Here 473 we sought to better understand this key processing step by imaging from major cell types in the 474 olfactory network and sampling odorants in the anesthetized mouse using a standard, 475 reproducible inhalation. This approach allowed us to compare the dynamics of inhalation-linked 476 activity as it progressed through the OB glomerular network, beginning with OSN inputs and 477 glomerular layer interneurons thought to perform key sensory processing early in the respiratory 478 cycle, and ending with mitral and tufted cells, which carry information out of the olfactory bulb. 479 Several general principles emerged. First, inhalation elicits relatively simple bursts of 480 OSN input to a glomerulus, which occur over a limited range of latencies that is glomerulus- and 481 odor-specific. Second, juxtaglomerular inhibitory interneurons – e.g., presumptive PG and SA 482 cells - also show uniformly short onset latencies and simple excitatory response transients 483 following inhalation. Third, diversity in inhalation-linked response patterns emerges at the level 484 of glomerular output neurons, manifesting in a larger range of times to peak response and burst 485 durations and in a higher prevalence of suppressive components of the inhalation-linked 486 response. Finally, we find that mitral and tufted cell response patterns are highly overlapping, 487 such that these projection neuron subtypes cannot be cleanly distinguished solely on the basis 488 of their inhalation-linked responses. Overall, these results are consistent with a model in which 489 diversity in inhalation-linked patterning of OB output arises first at the level of OSN inputs to the

OB and is then enhanced by feedforward inhibitory circuits in the glomerular layer (Dhawale et
al., 2010, Kikuta et al., 2013).

492 The glomerulus- and odorant-specific variation in inhalation-linked response latencies of 493 OSN inputs is consistent with that described earlier by us and others (Spors et al., 2006, Carey et al., 2009), with latencies varying across a range of 197 - 321 ms (25<sup>th</sup> - 75<sup>th</sup> percentiles). 494 495 Notably, PG and SA cells showed a near-identical distribution of response patterns, with 496 responses overwhelmingly consisting of simple and brief inhalation-driven bursts of excitation. 497 However, a fraction of SA cells displayed response durations that were prolonged relative to 498 those of PG cells. In contrast, diversity in inhalation-locked mitral and tufted cell activity could 499 not be fully accounted for by diversity in OSN inputs. Both mitral and tufted cell populations 500 displayed more delayed inhalation-linked onset latencies and larger range of time to peak and 501 burst durations than seen among OSNs, and inhalation-linked response patterns could include 502 multiphasic excitatory components - features which were rare or absent among OSNs.

503 Our data also allowed us to compare inhalation-linked response patterns of mitral versus 504 tufted cells. Surprisingly, at the population level, we found little difference in inhalation-linked 505 dynamics between these two populations. We did observe that the prevalence of clean air 506 evoked ITA responses was greater among sTCs. Furthermore, sTCs defined by their expression 507 of the neuropeptide transmitter CCK showed a significantly shorter range of response latencies 508 and durations than mitral cells or the wider population of sTCs. However, the distribution of sTC 509 and mitral cell response patterns overlapped a great deal: mitral and sTCs (as defined by soma 510 location regardless of genetic marker) were not different in mean onset latencies, and the mode 511 of their latency distribution was identical for the two cell types. Some earlier studies have 512 reported clear differences in the latencies of mitral versus tufted cell responses to inhalation of 513 air, although these timing differences disappear during odorant stimulation (Fukunaga et al., 514 2012, Fukunaga et al., 2014); thus our results are not inconsistent with these recent reports.

515 Finally, while relatively rare compared to earlier reports (Kollo et al., 2014, Economo et al., 516 2016, Diaz-Quesada et al., 2018), inhalation-linked suppression was seen in odorant responses 517 of both mitral cells and sTCs. Overall, our data are consistent with the long-held notion that 518 mitral and tufted cells constitute functionally distinct subpopulations of output neurons, but 519 indicate that these cell types cannot be distinguished solely on the basis of their inhalation-520 linked responses. Instead, our data suggest that the representation of olfactory information by 521 these subpopulations, at least with respect to the temporal dynamics of odor-evoked activity 522 following inhalation, is highly overlapping.

523 Respiratory patterning of ongoing activity in the absence of odorant stimulation is well-524 documented and has been hypothesized, among other functions, to serve as a reference for a 525 timing-based code for odor identity (Kepecs et al., 2006, Spors et al., 2006, Cury and Uchida, 526 2010, Shusterman et al., 2011, Wachowiak, 2011). Here, we observed inhalation-linked 527 patterning of activity during inhalation of clean air in all OB cell types, although the prevalence of 528 such responses (<10% across all populations) was smaller than reported in earlier studies 529 (Fukunaga et al., 2014, Diaz-Quesada et al., 2018). Indeed, in this study, excitation in response 530 to inhalation was unique to sTCs and not observed among MCs. This lower prevalence may be 531 a result of our use of cleaned air rather than ambient room air as our background condition, or 532 may reflect limitations in the sensitivity and temporal resolution of the GCaMP imaging 533 approach.

Surprisingly, a small fraction of clean air-driven responses were suppressive, with such suppression observed in sTCs, MCs and even some OSN inputs. To our knowledge, this is the first report of inhalation alone driving suppression of activity in these cell types. One explanation for these results could lie in the low frequency (0.25 Hz) of artificial inhalation used in our experiments: if some OSN populations are sensitive to odor components arising from within the animal's own nasal cavity – for example from metabolic processes - these components could

drive basal activity of OSNs and in sTCs of their target glomeruli, which would be transiently
removed by each inhalation of clean air. This effect could be even more pronounced in the
intact, awake mouse where OSNs are exposed to exhaled air containing metabolic odorants
(Munger et al., 2010, Mori et al., 2014).

544 What can we infer from these comparisons about the primary synaptic interactions 545 shaping inhalation-linked patterning of olfactory bulb output? First, the data suggest that PG and 546 SA cell excitation largely follows OSN input dynamics, consistent with evidence from slice 547 studies that these cells are highly sensitive to OSN stimulation mediated either by mono- or 548 disynaptic excitation (Gire and Schoppa, 2009, Shao et al., 2009, Kiyokage et al., 2010, Najac 549 et al., 2015). We saw little to no evidence of delayed PG/SA cell responses that would 550 correspond to feedback excitation from the late-phase responses observed in some MTCs. In 551 fact, only 2.3% of PG and 7.4% of SA interneuron onset latencies followed the mean M/sTC 552 onset latency. This result is somewhat surprising, as mitral cells can mediate feedback 553 excitation of PG and SA cells via dendrodendritic synapses in the glomerular neuropil (Najac et 554 al., 2015). Second, our results suggest that rapid feedforward inhibition from PG or SA cells may 555 underlie the longer-latency responses seen in some mitral and tufted cells – for example, the 556 slowest quartile of MT responses show onset latencies that roughly match the median peak time 557 of the PG cell response. Third, the presence of longer-duration mitral cell excitatory responses 558 that outlast those of any OSN input suggests an additional source of excitatory drive onto mitral 559 cells, the identity of which remains unclear. A disinhibitory circuit is unlikely, as we did not 560 observe suppression of PG or SA cells, therefore these results suggest that the intrinsic 561 properties of MT cells could give rise to prolonged spike bursts, or that secondary excitation by 562 ET cells could extend the duration of M/sTC excitatory responses (Carlson et al., 2000). This 563 prolonged excitatory component was often longer than the 4-second interval between sniffs,

implying that it may be important in shaping tonic levels of excitability across multiple inhalationsin the awake animal (Diaz-Quesada et al., 2018).

566 Overall, these results establish a basic framework for how glomerular circuits are 567 engaged to shape inhalation-linked patterning of olfactory bulb output. Our findings support the 568 hypothesis that feedforward inhibitory circuits can add to the initial diversity of temporal patterns 569 of input relayed by olfactory sensory neurons. Further experiments are necessary to integrate 570 other olfactory bulb cell types into this framework - for example, granule cells, deep short axon 571 cells, external plexiform layer interneurons and centrifugal inputs from the olfactory cortex may 572 also contribute to shaping respiratory patterning of olfactory bulb output. Understanding the 573 response dynamics of each of these cell types with respect to a single inhalation of odorant 574 should allow for a dynamic model of olfactory bulb network function across the fundamental unit 575 of information sampling in the olfactory system. Such a model may be used to yield insights into 576 olfactory processing across the full range of sampling frequencies used in the behaving animal.

eNeuro Accepted Manuscript

577

### 579 **REFERENCES**

- Adam Y, Livneh Y, Miyamichi K, Groysman M, Luo L, Mizrahi A (2014) Functional
   transformations of odor inputs in the mouse olfactory bulb. Frontiers in neural circuits
   8:129.
- Arneodo EM, Penikis KB, Rabinowitz N, Licata A, Cichy A, Zhang J, Bozza T, Rinberg D (2018)
   Stimulus dependent diversity and stereotypy in the output of an olfactory functional unit.
   Nature communications 9:1347.

Aungst JL, Heyward PM, Puche AC, Karnup SV, Hayar A, Szabo G, Shipley MT (2003) Centresurround inhibition among olfactory bulb glomeruli. Nature 426:623-629.

- Banerjee A, Marbach F, Anselmi F, Koh MS, Davis MB, Garcia da Silva P, Delevich K, Oyibo HK, Gupta P, Li B, Albeanu DF (2015) An Interglomerular Circuit Gates Glomerular Output and Implements Gain Control in the Mouse Olfactory Bulb. Neuron 87:193-207.
- Bozza T, McGann JP, Mombaerts P, Wachowiak M (2004) In vivo imaging of neuronal activity by targeted expression of a genetically encoded probe in the mouse. Neuron 42:9-21.
- Carey RM, Verhagen JV, Wesson DW, Pirez N, Wachowiak M (2009) Temporal structure of receptor neuron input to the olfactory bulb imaged in behaving rats. J Neurophysiol 101:1073-1088.
- Carlson GC, Shipley MT, Keller A (2000) Long-lasting depolarizations in mitral cells of the rat olfactory bulb. J Neurosci 20:2011-2021.
- Cury KM, Uchida N (2010) Robust odor coding via inhalation-coupled transient activity in the mammalian olfactory bulb. Neuron 68:570-585.
- Dana H, Chen TW, Hu A, Shields BC, Guo C, Looger LL, Kim DS, Svoboda K (2014) Thy1-GCaMP6 transgenic mice for neuronal population imaging in vivo. PLoS One 9:e108697.
- Dana H, Mohar B, Sun Y, Narayan S, Gordus A, Hasseman JP, Tsegaye G, Holt GT, Hu A, Walpita D, Patel R, Macklin JJ, Bargmann CI, Ahrens MB, Schreiter ER, Jayaraman V, Looger LL, Svoboda K, Kim DS (2016) Sensitive red protein calcium indicators for imaging neural activity. eLife 5.
- Dhawale AK, Hagiwara A, Bhalla US, Murthy VN, Albeanu DF (2010) Non-redundant odor coding by sister mitral cells revealed by light addressable glomeruli in the mouse. Nat Neurosci 13:1404-1412.
- Diaz-Quesada M, Youngstrom IA, Tsuno Y, Hansen KR, Economo MN, Wachowiak M (2018) Inhalation Frequency Controls Reformatting of Mitral/Tufted Cell Odor Representations in the Olfactory Bulb. J Neurosci 38:2189-2206.
- Economo MN, Hansen KR, Wachowiak M (2016) Control of Mitral/Tufted Cell Output by
   Selective Inhibition among Olfactory Bulb Glomeruli. Neuron 91:397-411.
  - Fukunaga I, Berning M, Kollo M, Schmaltz A, Schaefer AT (2012) Two distinct channels of olfactory bulb output. Neuron 75:320-329.
- Fukunaga I, Herb JT, Kollo M, Boyden ES, Schaefer AT (2014) Independent control of gamma
   and theta activity by distinct interneuron networks in the olfactory bulb. Nat Neurosci
   17:1208-1216.
- Geramita M, Urban NN (2017) Differences in Glomerular-Layer-Mediated Feedforward Inhibition
   onto Mitral and Tufted Cells Lead to Distinct Modes of Intensity Coding. J Neurosci
   37:1428-1438.
- 622 Gire DH, Schoppa NE (2009) Control of on/off glomerular signaling by a local GABAergic 623 microcircuit in the olfactory bulb. J Neurosci 29:13454-13464.
- 624 Grosmaitre X, Santarelli LC, Tan J, Luo M, Ma M (2007) Dual functions of mammalian olfactory 625 sensory neurons as odor detectors and mechanical sensors. Nat Neurosci 10:348-354.

586

587

588

589

590

591

592

593

594

595

596 597

598

599

600

601

602 603

604

605

606 607

608

609

610

611

614

neurons read out a relative time code in the olfactory bulb. Nat Neurosci 16:949-957. Homma R, Lv X, Sato T, Imamura F, Zeng S, Nagayama S (2019) Narrowly confined and glomerulus-specific onset latencies of odor-evoked calcium transients in the juxtaglomerular cells of the mouse main olfactory bulb. eNeuro ENEURO.0387-0318.2019. Igarashi KM, leki N, An M, Yamaguchi Y, Nagayama S, Kobayakawa K, Kobayakawa R, Tanifuji M, Sakano H, Chen WR, Mori K (2012) Parallel mitral and tufted cell pathways route distinct odor information to different targets in the olfactory cortex. J Neurosci 32:7970-7985. Johnson BN, Mainland JD, Sobel N (2003) Rapid olfactory processing implicates subcortical control of an olfactomotor system. J Neurophysiol 90:1084-1094. Kepecs A, Uchida N, Mainen ZF (2006) The sniff as a unit of olfactory processing. Chem Senses 31:167-179. Kepecs A, Uchida N, Mainen ZF (2007) Rapid and precise control of sniffing during olfactory discrimination in rats. J Neurophysiol 98:205-213. Kikuta S, Fletcher ML, Homma R, Yamasoba T, Nagayama S (2013) Odorant response properties of individual neurons in an olfactory glomerular module. Neuron 77:1122-1135. Kiyokage E, Pan YZ, Shao Z, Kobayashi K, Szabo G, Yanagawa Y, Obata K, Okano H, Toida K, Puche AC, Shipley MT (2010) Molecular identity of periglomerular and short axon cells. J Neurosci 30:1185-1196. Kollo M, Schmaltz A, Abdelhamid M, Fukunaga I, Schaefer AT (2014) 'Silent' mitral cells dominate odor responses in the olfactory bulb of awake mice. Nat Neurosci 17:1313-1315. Kosaka T, Kosaka K (2008) Tyrosine hydroxylase-positive GABAergic juxtaglomerular neurons are the main source of the interglomerular connections in the mouse main olfactory bulb. Neuroscience research 60:349-354. Laing DG (1986) Identification of single dissimilar odors is achieved by humans with a single sniff. Physiol Behav 37:163-170. Liu S, Plachez C, Shao Z, Puche A, Shipley MT (2013) Olfactory bulb short axon cell release of GABA and dopamine produces a temporally biphasic inhibition-excitation response in external tufted cells. J Neurosci 33:2916-2926. Liu SL, Puche AC, Shipley MT (2016a) The Interglomerular Circuit Directly Inhibits Mitral/tufted Cells. Chemical Senses 41:E35-E35. Liu SL, Puche AC, Shipley MT (2016b) The Interglomerular Circuit Potently Inhibits Olfactory Bulb Output Neurons by Both Direct and Indirect Pathways. Journal of Neuroscience 36:9604-9617. Liu WL, Shipley MT (1994) Intrabulbar associational system in the rat olfactory bulb comprises cholecystokinin-containing tufted cells that synapse onto the dendrites of GABAergic granule cells. J Comp Neurol 346:541-558. Macrides F, Chorover SL (1972) Olfactory bulb units: activity correlated with inhalation cycles and odor quality. Science 175:84-87. Mori K, Manabe H, Narikiyo K (2014) Possible functional role of olfactory subsystems in monitoring inhalation and exhalation. Frontiers in neuroanatomy 8:107. Munger SD, Leinders-Zufall T, McDougall LM, Cockerham RE, Schmid A, Wandernoth P, Wennemuth G, Biel M, Zufall F, Kelliher KR (2010) An olfactory subsystem that detects

Haddad R, Lanjuin A, Madisen L, Zeng H, Murthy VN, Uchida N (2013) Olfactory cortical

673 1444.
674 Nagai Y, Sano H, Yokoi M (2005) Transgenic expression of Cre recombinase in mitral/tufted
675 cells of the olfactory bulb. Genesis 43:12-16.

carbon disulfide and mediates food-related social learning. Current biology : CB 20:1438-

683

684

685

686

687

688

689

690

691

692

693

694

695 696

697

698

699

700

701

702

703

704

705

706

707

708

713 714

715

716

- Najac M, Sanz Diez A, Kumar A, Benito N, Charpak S, De Saint Jan D (2015) Intraglomerular 676 677 lateral inhibition promotes spike timing variability in principal neurons of the olfactory 678 bulb. J Neurosci 35:4319-4331.
- 679 Onoda N, Mori K (1980) Depth distribution of temporal firing patterns in olfactory bulb related to 680 air-intake cycles. J Neurophysiol 44:29-39.
- Pologruto TA, Sabatini BL, Svoboda K (2003) ScanImage: flexible software for operating laser 682 scanning microscopes. Biomedical engineering online 2:13.
  - Rebello MR, McTavish TS, Willhite DC, Short SM, Shepherd GM, Verhagen JV (2014) Perception of odors linked to precise timing in the olfactory system. PLoS biology 12:e1002021.
  - Schaefer AT, Angelo K, Spors H, Margrie TW (2006) Neuronal oscillations enhance stimulus discrimination by ensuring action potential precision. PLoS biology 4:e163.
  - Schaefer AT, Margrie TW (2007) Spatiotemporal representations in the olfactory system. Trends in neurosciences 30:92-100.
  - Seroogy KB, Brecha N, Gall C (1985) Distribution of cholecystokinin-like immunoreactivity in the rat main olfactory bulb. J Comp Neurol 239:373-383.
  - Shao Z, Puche AC, Kiyokage E, Szabo G, Shipley MT (2009) Two GABAergic intraglomerular circuits differentially regulate tonic and phasic presynaptic inhibition of olfactory nerve terminals. J Neurophysiol 101:1988-2001.
  - Shao Z, Puche AC, Liu S, Shipley MT (2012) Intraglomerular inhibition shapes the strength and temporal structure of glomerular output. J Neurophysiol 108:782-793.
  - Shirley CH, Coddington EJ, Heyward PM (2010) All-or-none population bursts temporally constrain surround inhibition between mouse olfactory glomeruli. Brain research bulletin 81:406-415.
  - Shusterman R, Smear MC, Koulakov AA, Rinberg D (2011) Precise olfactory responses tile the sniff cycle. Nat Neurosci 14:1039-1044.
  - Sobel EC, Tank DW (1993) Timing of odor stimulation does not alter patterning of olfactory bulb unit activity in freely breathing rats. J Neurophysiol 69:1331-1337.
  - Spors H, Wachowiak M, Cohen LB, Friedrich RW (2006) Temporal dynamics and latency patterns of receptor neuron input to the olfactory bulb. J Neurosci 26:1247-1259.
  - Sun Y, Nern A, Franconville R, Dana H, Schreiter ER, Looger LL, Svoboda K, Kim DS, Hermundstad AM, Jayaraman V (2017) Neural signatures of dynamic stimulus selection in Drosophila. Nat Neurosci 20:1104-1113.
- 709 Tobin VA, Hashimoto H, Wacker DW, Takayanagi Y, Langnaese K, Caguineau C, Noack J, 710 Landgraf R, Onaka T, Leng G, Meddle SL, Engelmann M, Ludwig M (2010) An intrinsic 711 vasopressin system in the olfactory bulb is involved in social recognition. Nature 464:413-712 417.
  - Uchida N, Mainen ZF (2003) Speed and accuracy of olfactory discrimination in the rat. Nat Neurosci 6:1224-1229.
  - Verhagen JV, Wesson DW, Netoff TI, White JA, Wachowiak M (2007) Sniffing controls an adaptive filter of sensory input to the olfactory bulb. Nature Neuroscience 10:631-639.
    - Wachowiak M (2011) All in a sniff: olfaction as a model for active sensing. Neuron 71:962-973.
- Wachowiak M, Cohen LB (2001) Representation of odorants by receptor neuron input to the 718 719 mouse olfactory bulb. Neuron 32:723-735.
- 720 Wachowiak M, Economo MN, Diaz-Quesada M, Brunert D, Wesson DW, White JA, Rothermel 721 M (2013) Optical dissection of odor information processing in vivo using GCaMPs 722 expressed in specified cell types of the olfactory bulb. J Neurosci 33:5285-5300.
- 723 Wachowiak M, Shipley MT (2006) Coding and synaptic processing of sensory information in the 724 glomerular layer of the olfactory bulb. Seminars in cell & developmental biology 17:411-725 423.

- Wesson DW, Carey RM, Verhagen JV, Wachowiak M (2008) Rapid encoding and perception of 726 727 novel odors in the rat. PLoS biology 6:e82.
- Wesson DW, Verhagen JV, Wachowiak M (2009) Why sniff fast? The relationship between sniff 728 729 frequency, odor discrimination, and receptor neuron activation in the rat. J Neurophysiol 730 101:1089-1102.
- Whitesell JD, Sorensen KA, Jarvie BC, Hentges ST, Schoppa NE (2013) Interglomerular lateral 731 732 inhibition targeted on external tufted cells in the olfactory bulb. J Neurosci 33:1552-1563. 733

### 736 Figure legends

737

### 738 Figure 1. Imaging inhalation triggered temporal dynamics of OB neuron subtypes.

A. Schematic of preparation for artificial inhalation in the anesthetized mouse. Inhalations were
 generated by a vacuum pulse applied to nasopharynx at 0.25 Hz.

B. Example resting fluorescence (left) and inhalation-triggered average (ITA) fluoresce change
 map taken from a glomerulus (glom.) and interneuron somata (soma) in the glomerular layer in

a GAD2-Cre:GCaMP6f reporter cross during odorant stimulation. White scale bar =  $50 \mu m$ .

Presumptive PG cell somata and glomerular boundaries are difficult to distinguish in the resting
 fluorescence image, but are clearly apparent in the response map.

C. Traces showing the fluorescence signal imaged from the glomerular neuropil and soma of an
associated GAD2+ neuron, from the example in (B). Traces show a typical imaging epoch, with
three 20s odor stimuli (grey) presented during 0.25 Hz inhalation (vertical lines).

749 D. Overlaid inhalation triggered calcium signals (top) and corresponding ITAs (middle) taken 750 from the glomerulus and soma during each inhalation in the presence of odorant. Dashed line 751 indicates inhalation onset. Bottom: Schematic illustrating definition of onset latency, time to 752 peak, and response duration. Onset latency was calculated from the ITA trace (solid black line) 753 when the response initially surpassed at least 4 consecutive frames, 4 standard deviations (SD) 754 above baseline. Time to peak (time to maximum response) and response duration (time 755 between the half max and half min points) were calculated from the ITA after applying the 756 Gaussian weighted box filter (dotted magenta line).

757

## Figure 2. Inhalation-linked dynamics of mitral and superficial tufted cells are diverse and highly overlapping.

760 A. GCaMP6f expression targeted to MC and sTC populations using reporter crosses to target 761 GCaMP6f expression in Tbx21+, CCK+, and Thy1+ MTC populations and virus injections into 762 the olfactory bulb to target GCaMP6f expression to PCdh21+ MTCs. Glomerular layer (GL), 763 external plexiform layer (EPL), and mitral cell layer (MCL) are labeled using dotted white lines. 764 B. Resting fluorescence (top) and odor-evoked ITA response maps (bottom) of sTCs imaged 765 from superficial EPL (left images) and MCs imaged from the mitral cell layer (right images). 766 Middle column shows ITA traces from sTCs (top) and MCs (bottom) indicated in the images. 767 Signals were low-pass filtered at 3 Hz prior to averaging and scaled relative to the pre-inhalation 768 baseline (i.e.,  $\Delta$  F/F). EPL and MCL images were taken from fields of view that were

- immediately above and below each other in the same Tbet-Cre: Rosa-GCaMP6f mouse during
- 570 stimulation with the same odorant (methyl valerate). All white scale bars = 50 μm.
- 771 C. Pseudo-color plots of ITA responses for all excitatory responses in sTC (top), MC (middle),
- and CCK+ sTCs (bottom); each row shows a different cell-odor pair. Each trace (row) was
- normalized to its own max and negative max amplitudes on a scale from -1 to 1. Red vertical
- line indicates inhalation onset.
- D. Box and whisker plots of sTC, MC, and CCK+ sTC onset latency distributions. Outliers
   marked with red dashes.
- E. Cumulative distribution plots of onset latency (top), time to peak (middle), and duration
  (bottom) for MC, sTCs, and CCK+ sTC ITAs.

## Figure 3. Diversity of inhalation-linked dynamics of mitral and superficial tufted cells within the same field of view.

- A. Resting fluorescence and odor-evoked ITA response map showing sTCs and MCs imaged in
   the same field of view using an oblique imaging plane in a Tbet-Cre: Rosa-GCaMP6f mouse
   during stimulation with methyl valerate. GI, glomerular neuropil.
- B. Traces showing ITAs from the sTCs and MCs shown in (A), illustrating temporal diversity of
   inhalation-linked responses across different cell types imaged simultaneously.
- 787 C. Plots comparing latency, peak time and duration of ITAs from sTCs (blue) and MCs (red)
- imaged in the same field of view or successive z-planes, allowing for paired comparisons (see
- Text). Black horizontal line spans the interquartile range. White scale bars, 50 μm.
- 790

779

### 791 Figure 4. Inhalation-linked suppression in mitral and superficial tufted cells.

A. Left: Odorant-evoked ITA response map including several MCs (Tbet-Cre: Rosa-GCaMP6f mouse) that show suppression of ongoing activity after each inhalation of odorant (methyl valerate, same preparation shown in Figure 2B), with ITA traces from each cell shown below. A
3 Hz low pass filter was applied to all traces prior to averaging. Right: Continuous traces from each MC showing fluorescence decrease after odorant inhalation, which is only apparent when ongoing activity (reflected in pre-odor fluorescence) is sufficiently high.
B. Same as in (A) but showing ITA responses of sTCs imaged from the superficial EPL in the

- same animal in (A). The field of view is directly above that shown in (A). The odorant is also the
- same as that in (A). Trace shows ITA and continuous recording from a suppressed sTC. This
- 801 cell was suppressed by inhalation and therefore the response is the same in the presence of 802 clean air or odorant. All white scale bars =  $50 \mu m$ .

### 804 Figure 5. Comparison of inhalation-linked dynamics of OSN inputs and MTCs.

A. GCaMP6f expression in OSN axons innervating OB glomeruli as seen in confocal histology in
 an OMP-Cre:Rosa-GCaMP6f mouse.

807 B. In vivo resting fluorescence (left) and odorant-evoked ITA response map imaged across

glomeruli of the dorsal OB. ITA response traces from the indicated glomeruli are shown at right.

Note the range of excitatory dynamics and the presence of a suppressive response in oneglomerulus.

C. Odor-evoked ITA response maps (left) and traces (right) showing three glomeruli that each
 respond to two odorants: methyl valerate (MV) and 2-methyl pentanal (2-MP).

D. ITA traces for each odorant are overlaid for the same glomerulus, illustrating odorant-specificresponse dynamics.

815 E. Pseudocolor plots of ITA responses for all odor-glomerulus pairs, displayed and normalized,

as in Figure 2, to their minimum (-1) and maximum (1) amplitude response. Red vertical lineindicates inhalation onset.

818 F. Cumulative distribution plots showing OSN ITA onset latencies, times to peak, and durations,

with the values for MCs, sTCs, and CCK+ sTCs (same data as in Figure 2) included for
comparison. All scale bars, 100 μm.

## Figure 6. Juxtaglomerular interneurons show simple and short-latency responses toodorant inhalation.

A. GCaMP6f expression in the glomerular layer of a GAD2-IRES-Cre mouse, showing
expression in juxtaglomerular neurons with extensive processes in the glomerular layer (GL).
Scale bar, 50 µm.

827 B. In vivo resting fluorescence (left) and odorant-evoked ITA response map (right) showing

828 activation of two adjacent glomeruli in a GAD2-Cre: Rosa GCaMP6f mouse. Note that numerous

somata are apparent around the periphery of the right glomerulus in the response map.

Numbers indicate somata whose ITAs are shown in (C). GI, glomerular neuropil. Scale bar, 50
µm. Odorant was methyl valerate.

C. ITA traces from the somata and glomerular neuropil from (B). Traces were low-pass filtered
at 5Hz prior to averaging. The same traces are shown scaled to the same peak values at right.

Note that all cells show similar onset latencies with only modest differences in time to peak orduration.

821

D-F. Similar to (A-C), but for dopaminergic neurons using a DAT-Cre: Rosa GCaMP6f mouse to
target presumptive SA cells. The ITA traces for these DAT+ cells are also all short-latency, with
one cell showing a longer-lasting response. Odorant was 2-Hexanone. Scale bar in (D), 30 µm.
Scale bar in (E), 50 µm.
G. Pseudocolor plots of ITA responses for all cell-odor pairs for GAD2+/presumptive PG cells

841 (top) and DAT+/TH+ presumptive SA cells (bottom), displayed and normalized as in Figure 2.
842 Red vertical line indicates inhalation onset.

H. Box plot comparisons of ITA onset latencies, time to peak, and half width durations. Medians e center horizontal line. Boxes represent  $2^{nd}$  and  $3^{rd}$  quartiles of each cell populations.

845 I. Cumulative distribution plots of onset latencies, times to peak, and durations for GAD2+ and

B46 DAT/TH+ cells highlighted by thicker plots. OSN and MTC populations shown for reference.
847

## Figure 7. Diversity of inhalation-linked temporal dynamics is greater in sTC than PG cells innervating the same glomerulus.

A. Tissue sections showing GCaMP6f expression (green) in Thy1+ MTCs (green) and

jRGECO1a expression in GAD2+ juxtaglomerular neurons, after Flex.jRGECO1a (red) virus
 injection in a Thy1-GCaMP6f:GAD2-Cre mouse (see Text). Scale bar, 100 µm.

853 B. Odorant-evoked ITA response map showing activation of MTCs recorded in the green

channel (top) and GAD2+ neurons recorded simultaneously in the red channel (bottom).

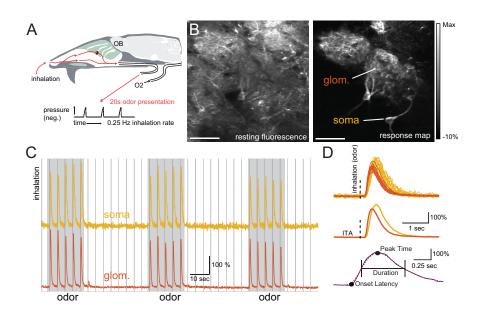
Numbers indicate presumed sTCs or PG cells whose responses are shown in (D). Odorant was
ethyl butyrate. Scale bar, 50 μm.

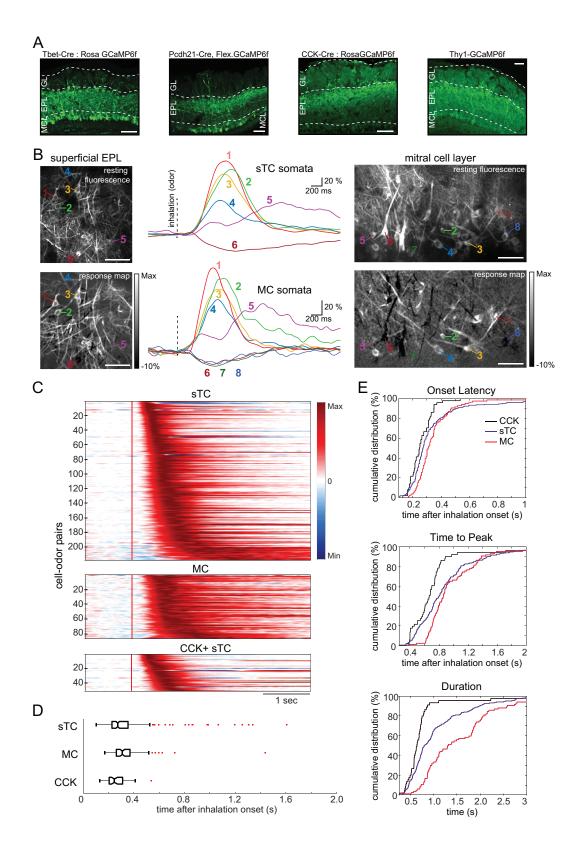
C. Overlay of ITA traces for the Thy1+ and GAD2+ signals recorded from the neuropil of the
glomerulus shown in (B). Traces normalized to their maximum response to highlight temporal
differences.

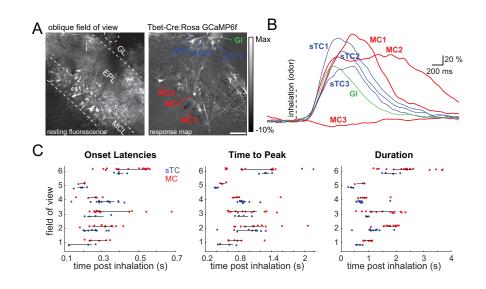
D. ITA traces from the somata indicated in (B), with presumptive sTCs (top) and PG cells
(bottom) overlaid with each other. All cells appear to innervate the same glomerulus. A 5 Hz low
pass filter was applied to all traces prior to averaging. Traces normalized to their maximum
response.

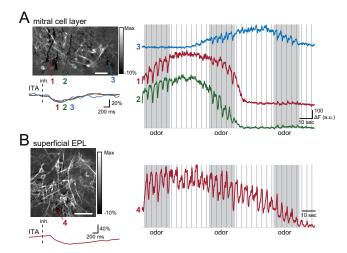
E. Resting fluorescence (left) and odorant-evoked ITA response map (right) taken from a TbetCre mouse expressing GCaMP6f, showing a group of sister sTCs innervating the same
glomerulus. Odorant was methyl valerate. Scale bar, 50 μm.

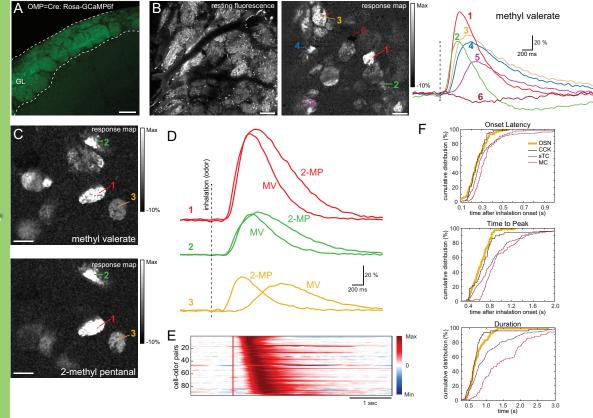
- 867 F. ITA response traces from the sTCs shown in (E), along with the glomerular signal (GL).
- 868 Traces shown at right are normalized to their peak response to illustrate diversity in inhalation-
- 869 linked rise-times and durations.
- 870 G. Dot plots showing the distribution of onset latencies for sister PG cells (left) or sTCs (right)
- 871 associated with the same glomerulus, referenced to the latency measured from the neuropil of
- the parent glomerulus (vertical line). Each row is a different glomerulus. Black horizontal line
- spans the interquartile range and the black asterisk is the median.
- H. Same analysis in (G) but for time to peak for the same cells and glomeruli.



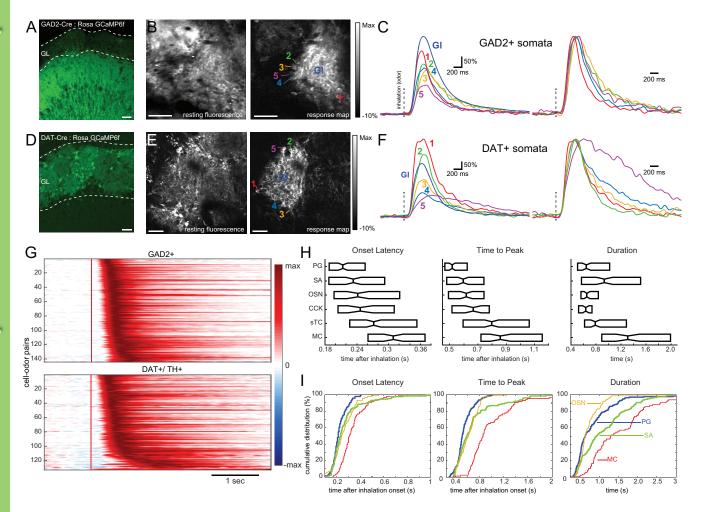








# eNeuro Accepted Manuscript



## eNeuro Accepted Manuscript

